



RESEARCH LETTER

10.1029/2026GL122395

Northern Hemisphere Wintertime Stratospheric Circulation Response to Smoke Injection From a Regional Nuclear Conflict

Key Points:

- Heat and momentum budget analyses reveal the mechanisms linking the aerosol perturbations to early stratospheric circulation responses
- During the first month after injection, aerosol radiative heating is confined to the tropical-subtropical stratosphere
- Dynamical processes play a key role in temperature changes over the mid-to-high latitudes as well as strengthening of the polar vortex

Supporting Information:

Supporting Information may be found in the online version of this article.

Correspondence to:

S. Yook,
syook@mit.edu

Citation:

Yook, S., Stone, K., Kang, J. M., Hwang, J., Zhuo, Z., & Pausata, F. S. R. (2026). Northern Hemisphere wintertime stratospheric circulation response to smoke injection from a regional nuclear conflict. *Geophysical Research Letters*, 53, e2026GL122395. <https://doi.org/10.1029/2026GL122395>

Received 11 FEB 2026

Accepted 9 MAY 2026

Simchan Yook¹ , Kane Stone¹ , Joonsuk M. Kang², Jaeyoung Hwang^{3,4} , Zhihong Zhuo⁵ , and Francesco S. R. Pausata⁵

¹Department of Earth, Atmospheric and Planetary Sciences, Massachusetts Institute of Technology, Cambridge, MA, USA, ²Columbia University, New York, NY, USA, ³Georgia Institute of Technology, Atlanta, GA, USA, ⁴Hankuk University of Foreign Studies, Seoul, South Korea, ⁵University of Quebec in Montreal, Montreal, QC, Canada

Abstract Tropical stratospheric aerosol injections are known to strengthen the wintertime Stratospheric Polar Vortex (SPV). Here, we revisit the circulation response to aerosol perturbations during the first month following injection using chemistry-climate model simulations of regional nuclear war scenarios. We diagnose the atmospheric heat and momentum budgets to assess the thermal and dynamical responses to tropical soot injection. The results reveal that, during the initial adjustment period of 30 days, radiative heating from aerosols is confined to the tropics. In contrast, temperature and circulation changes in the mid-to-high latitudes are governed primarily by dynamical processes, with changes in eddy momentum fluxes driving the intensification of the SPV. Together, these findings demonstrate that circulation responses to stratospheric aerosol perturbations—through the redistribution of heat and momentum to remote regions—play a key role in the strengthening of the winter polar jet.

Plain Language Summary Large injections of aerosols into the stratosphere are known to strengthen the winter polar vortex, but the physical processes responsible for this response are not fully understood. Using a climate model simulation of a regional nuclear war, we examine how the atmosphere responds during the first month after smoke particles are injected into the stratosphere. We find that warming from aerosol heating in this early period occurs mainly in the subtropics, while changes in atmospheric circulation transport this heat toward mid-latitudes. These circulation changes also modify atmospheric momentum transport, leading to a stronger polar jet. Our results show that atmospheric dynamics play a key role in how aerosol perturbations affect remote regions and strengthen the winter polar vortex.

1. Introduction

Observational studies have suggested that the Northern Hemisphere (NH) stratospheric polar vortex (SPV) tends to strengthen during boreal winters following major tropical volcanic eruptions (Graf et al., 2007; Kodera, 1995). The linkage between NH wintertime atmospheric circulation and stratospheric aerosol injections has also been extensively examined in numerical modeling studies across a range of contexts. Simulations of explosive volcanic eruptions (Bittner et al., 2016; DallaSanta et al., 2019; Graft et al., 1993) and geoengineering scenarios (Banerjee et al., 2021; Jones et al., 2021) typically implement massive injections of sulfur dioxide into the stratosphere. Nuclear war scenarios consider large injections of black carbon (BC) and organic carbon (OC) from urban fires (Coupe & Robock, 2021; Pausata et al., 2016). Results from several of these studies consistently indicate a broadly similar outcome: aerosol-induced heating of the tropical stratosphere followed by a strengthening of the SPV.

A variety of radiative and dynamical mechanisms have been proposed to explain the linkage between tropical aerosol perturbations and the strength of the SPV. In the following, temperature and circulation anomalies occurring locally adjacent to the aerosol plume are referred to as the direct response to aerosol perturbations.

1. *Stratospheric Gradient Mechanism*: The first mechanism involves warming of the tropical stratosphere due to aerosol-induced heating, which enhances the meridional temperature gradient and thereby strengthens the stratospheric jet through thermal wind balance (Coupe & Robock, 2021; Graft et al., 1993; Kodera, 1994; Robock & Mao, 1995).

© 2026. The Author(s).

This is an open access article under the terms of the [Creative Commons](#)

[Attribution-NonCommercial-NoDerivs](#)

License, which permits use and distribution in any medium, provided the original work is properly cited, the use is non-commercial and no modifications or adaptations are made.

2. *Wave Feedback Mechanism:* Other studies suggest that the changes in the stratospheric temperature gradient from the direct radiative effects of aerosol are largely confined to the subtropics (Bittner et al., 2016; Stenchikov et al., 2002; Toohey et al., 2014). Thus, the acceleration of the jet required to maintain thermal wind balance occurs mainly in the subtropical latitudes rather than the polar latitudes. The second mechanism has been proposed to explain the strengthening of the SPV through an indirect dynamical process. The eastward acceleration of the zonal wind fields in the subtropical stratosphere deflects planetary wave propagation equatorward (i.e., limits poleward wave fluxes), thereby indirectly intensifying the SPV (Bittner et al., 2016; DallaSanta et al., 2019; Toohey et al., 2014).
3. *Tropospheric Gradient Mechanism:* The third mechanism includes an indirect tropospheric pathway. Aerosol scattering of shortwave radiation cools the surface, weakens the tropospheric meridional temperature gradient and baroclinicity, which in turn, reduces upward wave flux and contributes to the polar jet acceleration (DallaSanta et al., 2019; Graft et al., 1993; Stenchikov et al., 2002).

Together, these mechanisms highlight how coupled radiative and dynamical adjustments can strengthen the wintertime SPV following tropical aerosol injections. However, it remains unclear whether these mechanisms operate on short timescales immediately after injection. Most previous work has focused on seasonal or longer-term responses, while the initial evolution of the circulation anomalies during the weeks immediately following injection—the period when the atmosphere adjusts most rapidly—remains relatively unexplored.

Here, we use a chemistry-climate model to examine how radiative and dynamical processes contribute to the stratospheric response to smoke injection in regional nuclear-war scenarios during the first month. We quantify the evolution of the heat and momentum budgets to assess the processes that link the initial aerosol perturbations to the early stage circulation responses.

2. Data and Methods

2.1. Model and Scenarios

We evaluate the Whole Atmosphere Community Climate Model version 4 (WACCM4, Marsh et al., 2013) simulations, previously run by Yook et al. (2025) to assess the climate response to a regional nuclear conflict. The simulations are run with fully interactive chemistry and coupled ocean, land, and sea-ice components, with a horizontal resolution of $1.9^\circ \times 2.5^\circ$, 66 vertical levels, and a model top near 140 km. The model incorporates the Model for Ozone and Related Chemical Tracers (Kinnison et al., 2007) and computes photolysis rates using the Tropospheric Ultraviolet and Visible radiation scheme (Madronich & Flocke, 1997), allowing for the effects of aerosol scattering and absorption on actinic fluxes.

Two sets of simulations are analyzed: (a) a control (*CTRL*) case with present-day background conditions and (b) an India-Pakistan (*IP*) case representing a regional nuclear conflict scenario following Yook et al. (2025). In the *IP* experiment, ~ 6.7 Tg of smoke (5 Tg BC and 1.7 Tg OC) is injected into the upper troposphere (150–300 hPa) over the India and Pakistan regions during 12–15 January of the first simulation year. The smoke aerosols are simulated with the Community Aerosol and Radiation Model for Atmospheres (CARMA, Bardeen et al., 2008), which explicitly represents coagulation, wet and dry deposition, and gravitational settling. Details of the model configuration and experimental design are described in Bardeen et al. (2021) and Yook et al. (2025). To focus on the radiative effects of smoke particles during the first month and to minimize feedback from substantial ozone depletion due to halogen chemistry reported in Yook et al. (2025), we did not include halogen emissions in this study.

Each set of experiments includes 16 ensemble members, initialized from different initial conditions on 1 January. The results presented here are based on the ensemble mean of each field to isolate circulation responses to stratospheric aerosol forcing from internal climate variability. All ensemble members were integrated for 4 months. In this study, we focus on the first month of the 4-month simulations because the changes in temperature tendency in response to the nuclear-war forcing are largest during the first month. The *IP* regional conflict scenario follows that described in Toon et al. (2019), in which no urban targets are attacked on the first day of the conflict. Accordingly, the first monthly average is calculated from day 1 of the war scenario (11 January), rather than from the first day on which urban targets are attacked (12 January).

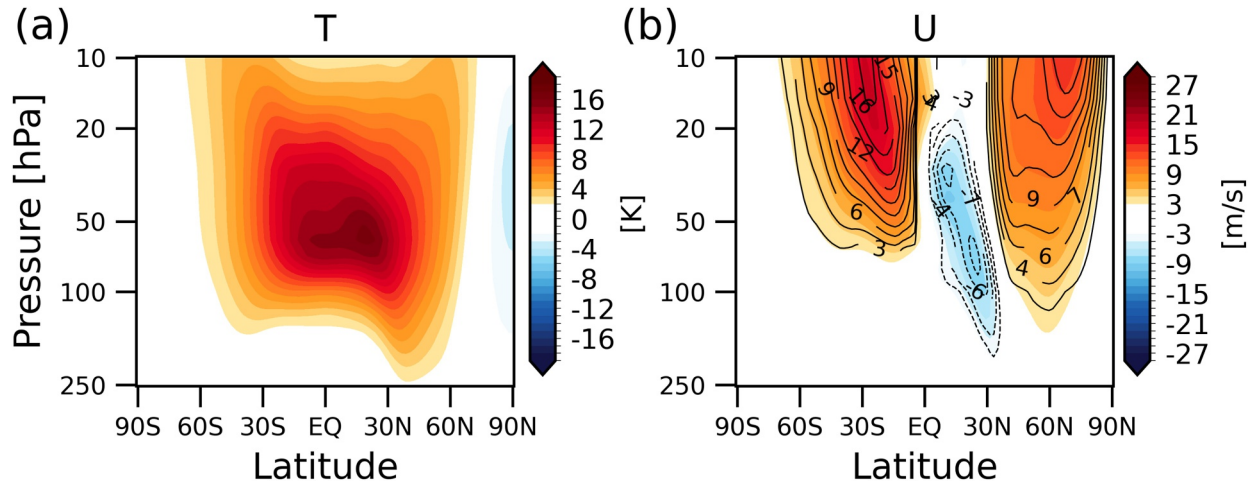


Figure 1. Changes in zonal-mean (a) temperature and (b) zonal wind between *IP* and *CTRL* simulations (color shading). In panel (b), line contours indicate zonal wind changes estimated from the thermal wind relationship using the temperature anomalies shown in panel (a). All fields are averaged over the 30-day period following the *IP* conflict from 11 January to 9 February.

2.2. The Zonal Mean Heat Budget

To assess the thermal and dynamical responses of the circulation, we quantify the temporal and spatial evolution of the stratospheric heat budget as a function of latitude and pressure (e.g., Holton, 2004; Lachmy & Kaspi, 2020; White et al., 2024). The prognostic equation for zonal mean temperature can be written as:

$$\underbrace{\frac{\partial \bar{T}}{\partial t}}_{\text{TEND}} = \underbrace{\bar{Q} - \bar{\omega}}_{\text{RAD}} \left(\underbrace{\frac{\partial \bar{T}}{\partial p}}_{\text{ADIA}} - \kappa \frac{\partial \bar{T}}{p} \right) - \underbrace{\frac{1}{a \cos \phi} \frac{\partial (\cos \phi \overline{v'T'})}{\partial \phi}}_{\text{EHFC}} - \left\{ \underbrace{\left(\frac{\partial (\overline{\omega'T'})}{\partial p} - \kappa \frac{(\overline{\omega'T'})}{p} \right)}_{\text{RES}} - \bar{v} \frac{\partial \bar{T}}{\partial \phi} + \overline{Q_{\text{GW}}} \right\} \quad (1)$$

Here, T is temperature, v is meridional wind, ω is vertical velocity in pressure coordinates, Q is the diabatic heating tendency, and Q_{GW} represents the heating rate due to gravity-wave drag. p is pressure, ϕ is latitude, a is Earth's radius, and $\kappa = R_d/c_p$. The overbar denotes the zonal mean, and the prime denotes deviations from the zonal mean.

The term on the left-hand side of the above equation represents the net temperature tendency (TEND). The first term on the right-hand side represents the diabatic heating from the sum of longwave and shortwave heating rates (i.e., radiative processes; RAD). The second term represents the adiabatic process by vertical motion (hereafter ADIA), and the third term corresponds to the meridional eddy heat flux convergence (EHFC). The remaining terms (fourth through sixth) represent heating due to vertical EHFC, temperature advection by the zonal mean meridional wind, and heating from gravity wave drag, respectively, comprising the residual terms (RES). To distinguish heating from dynamical processes from that due to radiative processes, we define the dynamical temperature tendency (DYN) as the sum of the ADIA, EHFC, and RES terms. Note that DYN refers only to dynamical processes in the temperature budget (Equation 1), not in the zonal-momentum budget (Equation 2), which will be discussed later.

3. Results

3.1. Stratospheric Temperature and Circulation Responses

The stratospheric climate anomalies during the first month after the *IP* conflict show a rapid warming after the injection, with temperature anomalies exceeding 15 K in the tropical lower stratosphere during the first month (Figure 1a). This tropical warming arises primarily from shortwave absorption by smoke particles, consistent with earlier studies of nuclear-conflict scenarios (Bardeen et al., 2021; Mills et al., 2008, 2014; Robock et al., 2007; Yook et al., 2025).

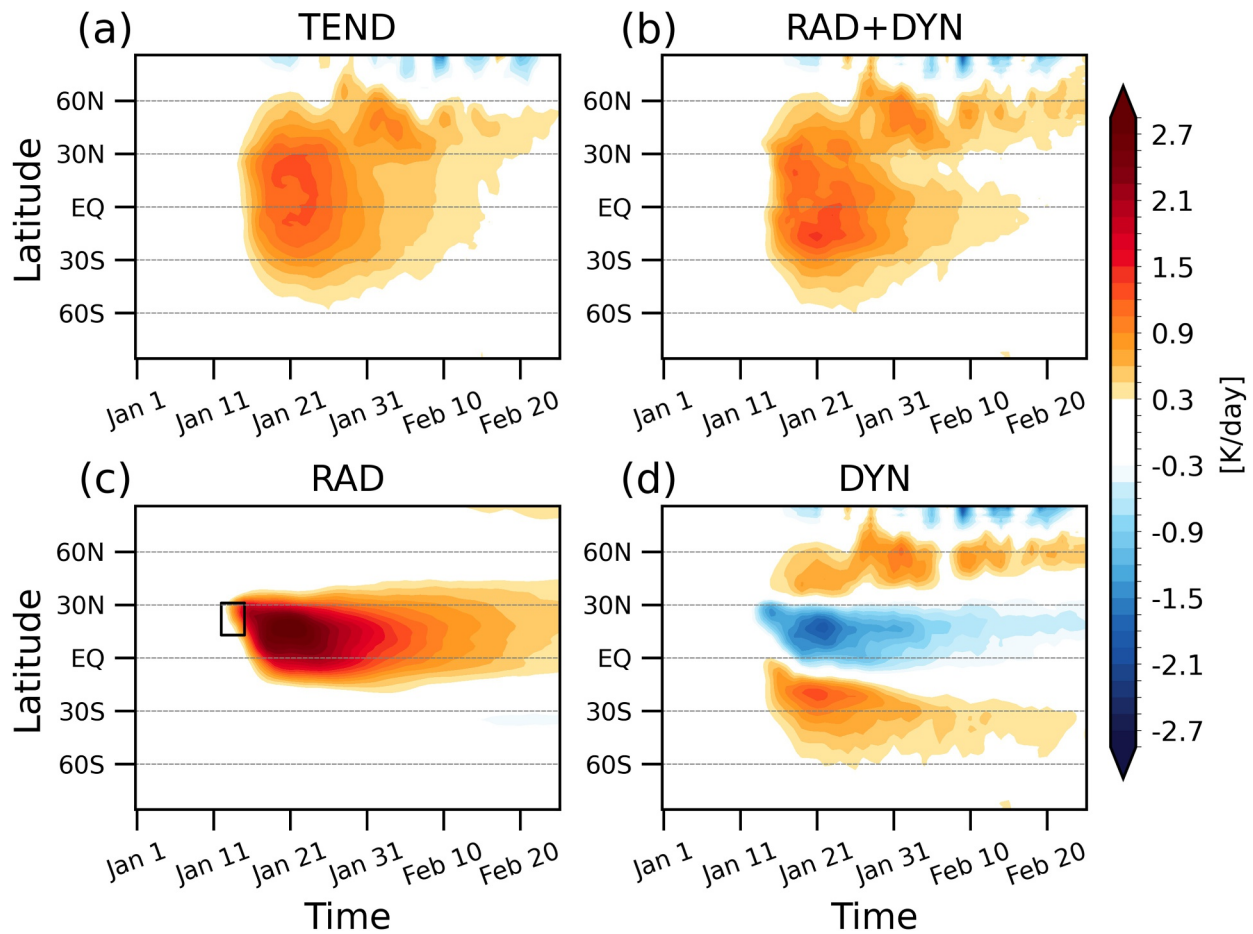


Figure 2. Time series of changes in stratospheric temperature tendency (K day^{-1}). Each panel shows (a) total temperature tendency (TEND and LHS of Equation 1), (b) sum of all diagnosed thermodynamic tendency terms (RAD + DYN and RHS of Equation 1). (c) Radiative heating term (RAD) and (d) dynamical contribution (DYN). The results are vertically averaged between the 100 and 10 hPa levels, with each layer weighted by pressure. All results in this figure, Figures 3 and 4 are shown as differences between the *IP* and *CTRL* simulations. Gray dashed lines indicate key latitudes (60°S , 30°S , equator, 30°N , 60°N) for reference. The black box in panel (c) marks the aerosol injection time and location for the *IP* conflict scenario.

The circulation responses are marked by strengthening of the wintertime SPV. Zonal wind anomalies show robust westerly accelerations across the NH mid-to-high latitudes as well as over the SH subtropics (Figure 1b). The thermal-wind response derived from the temperature anomalies (line contours) closely matches the simulated wind response (shading), indicating that the circulation anomalies are largely in thermal-wind balance with the temperature anomalies (Figure 1b). We further examine the processes contributing to the SPV intensification by quantifying the associated heat-budget in the next section.

3.2. Stratospheric Heat Budget Analyses

The evolution of stratospheric temperature following aerosol injection is quantified using the temperature tendency budget (Equation 1). The net temperature tendency across the global stratosphere (Figure 2a) is well captured by the sum of the diagnosed radiative and dynamical terms (Figure 2b), indicating that the heat-budget analysis accurately captures the processes driving the temperature response. The atmosphere warms rapidly over the tropics within a few days of the injection (12–15 January), and a secondary warming signal emerges in the extratropics roughly 2 weeks later.

The radiative and dynamical contributions to the temperature tendency exhibit distinct spatial structures (Figures 2c and 2d). Radiative heating produces strong tropical warming, consistent with shortwave absorption by smoke particles, but this radiative signal remains confined largely within $\pm 30^\circ$ latitude (Figure 2c). Radiative warming tendency of the tropical stratosphere peaks at $\sim 3 \text{ K day}^{-1}$ within the first week following the smoke

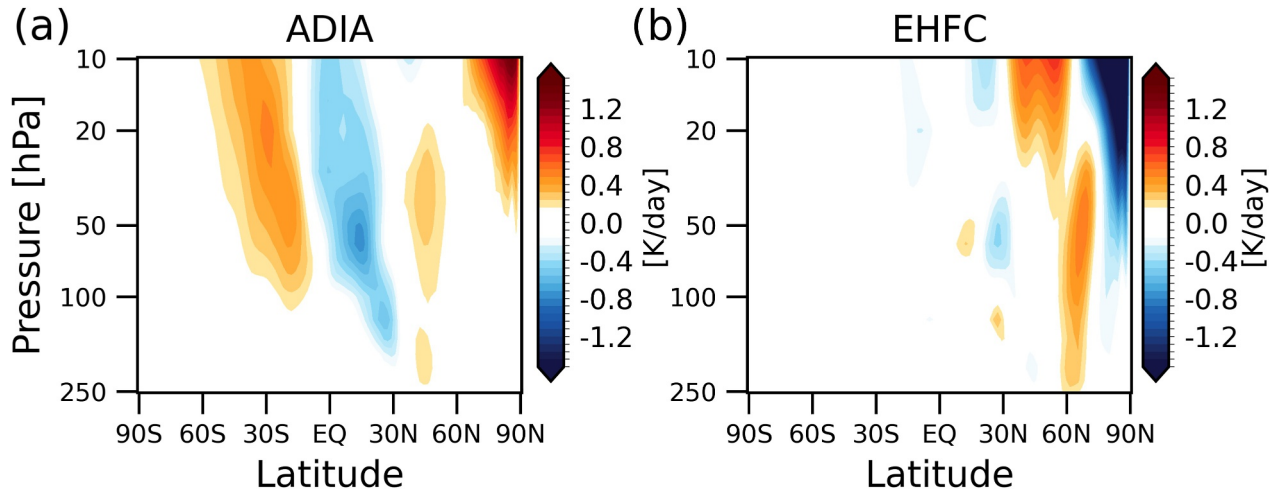


Figure 3. Zonal-mean temperature tendencies associated with (a) adiabatic process (ADIA) and (b) meridional eddy heat-flux convergence. All fields are averaged over the 30-day period following the IP conflict from 11 January to 9 February.

injection, but then declines to less than $\sim 1 \text{ K day}^{-1}$ over the course of a month. This indicates that the tropical stratosphere rapidly approaches radiative equilibrium, as the aerosol-induced heating is offset by enhanced longwave cooling from the Planck feedback.

The dynamical tendency exhibits cooling over the tropics and warming over the midlatitudes in both hemispheres (Figure 2d). The tropical cooling is associated with enhanced ascent and adiabatic cooling (Figure 3a and Figure S1a in Supporting Information S1) and the mid-to-high latitudes warming arises from both vertical motion (ADIA) and meridional heat transport by atmospheric eddies (EHFC) (Figure 3b and Figure S1b in Supporting Information S1). Warming associated with meridional eddy heat-flux convergence is evident across the stratosphere around $\sim 60^\circ\text{N}$, underscoring the importance of atmospheric eddies in shaping extratropical temperature anomalies (Figure 3b).

The sum of the ADIA and EHFC terms in Equation 1 (i.e., the DYN term when the RES term is neglected due to its small contribution) can be interpreted as the temperature tendency driven by the vertical component of the Transformed Eulerian mean (TEM) residual circulation (Text S1 in Supporting Information S1). Thus, negative anomalies of the DYN term are analogous to anomalous upward residual circulation, and vice versa. The DYN term also provides a clear representation of the net temperature change due to dynamical processes by removing the cancellation between the ADIA and EHFC terms (Figures S1 and S2 in Supporting Information S1).

Taken together, the results indicate that aerosol perturbations influence the temperature field through two pathways: (a) direct radiative heating in the tropics and (b) dynamical heat redistribution that transports warm anomalies poleward. The latter dominates the temperature anomalies at mid-to-high latitudes and highlights the key role of dynamical processes in driving the extratropical response to smoke injection.

3.3. Mechanisms for Stratospheric Polar Vortex Response

To further diagnose the circulation response, we examine the zonal-mean momentum budget as follows (Equation 2, Dima et al., 2005; Holton, 2004; White et al., 2024):

$$\frac{\partial \bar{U}}{\partial t} \cong \underbrace{\bar{v} \left(f - \frac{1}{a \cos \phi} \frac{\partial (\bar{u} \cos \phi)}{\partial \phi} \right)}_{\text{COR}} - \underbrace{\frac{1}{a \cos^2 \phi} \frac{\partial (\cos^2 \phi \overline{u'v'})}{\partial \phi}}_{\text{EMFC}} - \underbrace{\left(\bar{\omega} \frac{\partial \bar{u}}{\partial p} + \frac{\partial (\bar{u}'\omega')}{\partial p} - \bar{F}_r \right)}_{\text{URES}} \quad (2)$$

The wind tendency can be written as the sum of three terms, the Coriolis acceleration (for simplicity, including the meridional advection term associated with curvature effect; COR), the eddy momentum flux convergence (EMFC), and the residual term (URES), which includes vertical advection, vertical EMFC, and friction (F_r).

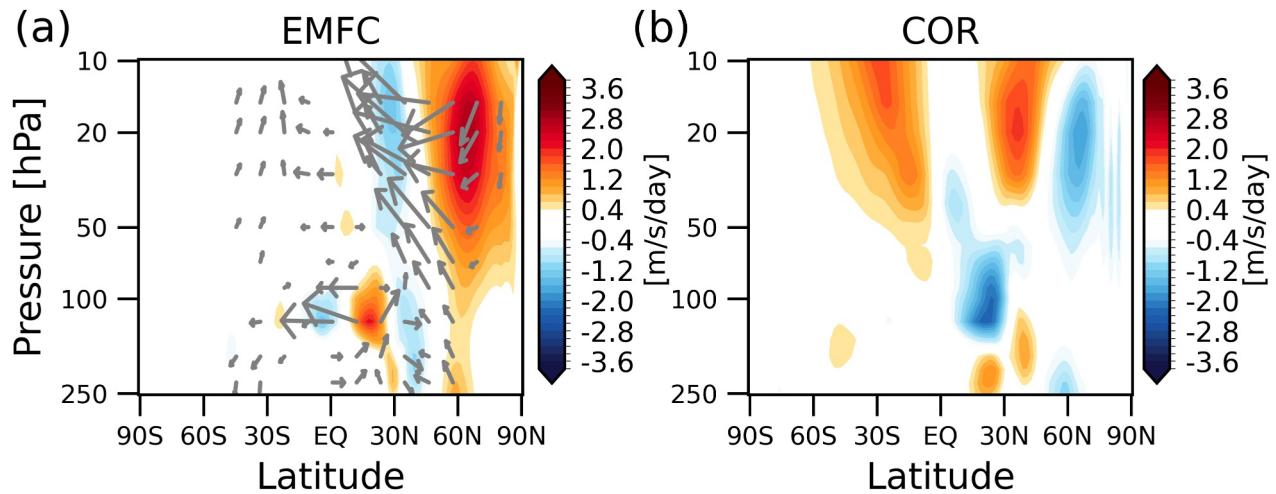


Figure 4. The acceleration of the zonal-mean zonal flow ($\text{m s}^{-1} \text{day}^{-1}$) associated with the (a) eddy momentum-flux convergence and (b) Coriolis torque (COR). All fields are averaged over the 30-day period following the IP conflict from 11 January to 9 February.

Figure 4 demonstrates the key components of the zonal-mean momentum budget that drive the anomalous zonal wind responses. The eddy momentum-flux convergence produces strong westerly accelerations throughout the stratosphere across $\sim 40^{\circ}\text{N}$ – 90°N (Figure 4a), indicating that eddy forcing is the primary driver of the anomalous zonal wind response. The spatial structure of the EMFC anomalies aligns with the regions of strengthened westerlies in Figure 1b. We note that EMFC represents large-scale Rossby wave forcing, which is a key driver of polar vortex variability (Newman et al., 2001; Waugh et al., 2017).

The EMFC anomalies are proportional to the divergence of the meridional component of the Eliassen-Palm flux (EPy) which provide a useful diagnostic for meridional propagation of planetary waves. The EPy anomalies show pronounced negative values over the NH midlatitudes, indicating enhanced equatorward wave propagation (Figure S2 in Supporting Information S1). As a result, wave breaking at high latitudes is reduced, which in turn weakens the deceleration of the SPV. These changes in enhanced equatorward wave propagation are consistent with findings from stratospheric aerosol-injection studies (Bittner et al., 2016; Coupe & Robock, 2021; Toohey et al., 2014). These results are also consistent with earlier dynamical studies of the circulation response to thermal perturbations in the tropical stratosphere, which showed that changes in horizontal eddy momentum fluxes play a crucial role in driving the midlatitude zonal wind anomalies (Haigh et al., 2005; Simpson et al., 2009).

The Coriolis torque—westerly torques associated with poleward wind anomalies—contributes more modestly to the zonal wind anomalies over the NH mid-to-high latitudes, indicating a slight equatorward shift of the zonal wind anomalies. The influence of the Coriolis torque is more pronounced over the SH subtropics and midlatitudes, where the jet intensifies but the EMFC anomalies are weak (Figure 4b). Overall, the results in Figure 4 reveal the dynamical pathway for the polar-jet acceleration, highlighting the key role of eddy momentum forcing via wave-mean flow interactions.

From the perspective of the TEM framework, the EMFC term (including its negative sign) is analogous to the meridional component of the EP flux divergence term (Text S1 and Figure S3c in Supporting Information S1), while the COR term can be decomposed into the sum of (a) the meridional component of the TEM circulation (Figure S3a in Supporting Information S1) and (b) the vertical component of the EP flux divergence term (Figure S3b in Supporting Information S1). The zonal-wind acceleration associated with the Eulerian (Figure 4b) and TEM (Figure S3a in Supporting Information S1) meridional velocities exhibits qualitatively similar structures, except at NH high latitudes. The westward acceleration near $\sim 60^{\circ}\text{N}$ in the Eulerian framework (Figure 4b), driven by anomalous southward meridional winds, can be attributed to wave-driven deceleration of the westerlies via the vertical component of the EP flux divergence (Figure S3b in Supporting Information S1). Consequently, the TEM framework shows weaker eastward anomalies over the NH polar region (Figure S3a in Supporting Information S1). Nevertheless, the acceleration of the polar vortex near $\sim 60^{\circ}\text{N}$ is primarily governed by the EMFC term in (Figure 4b or Figure S4c in Supporting Information S1), and is not sensitive to the choice of Eulerian or TEM framework.

4. Conclusions

This study uses a chemistry-climate model to examine the wintertime circulation response to smoke aerosol injected into the tropical stratosphere over the India-Pakistan region during a regional-scale nuclear conflict (for the exact emission locations please refer to Figure S1 in Yook et al. (2025)). We quantify the stratospheric heat and momentum budgets to assess the transient thermal and dynamical responses of the circulation to the aerosol perturbations. The heat budget reveals that tropical warming is driven by radiative heating, whereas extratropical warming arises primarily from dynamical processes that redistribute tropical heat poleward (Figure 2). These extratropical warm anomalies are largely driven by dynamical processes, primarily by meridional eddy heat flux (Figure 3). The momentum budget (Figure 4) further shows that the associated changes in eddy momentum-flux convergence play a key role in the strengthening of the polar vortex. Taken together, our results demonstrate how stratospheric aerosol perturbations influence atmospheric circulation in remote regions. Changes in atmospheric eddies in response to the aerosol perturbation play a key role in driving extratropical circulation anomalies through the redistribution of heat and momentum.

Previous studies have identified key mechanisms linking stratospheric aerosol injections to polar vortex strengthening: (a) the stratospheric gradient mechanism, (b) the wave-feedback mechanism, and (c) the tropospheric gradient mechanism, primarily based on analyses over seasonal to longer timescales. In this study, we focus on the initial ~30-day atmospheric response following the aerosol injection, a period sufficient for stratospheric temperature anomalies to approach radiative equilibrium (Figure 2). We clarify how these mechanisms operate on such short timescales by explicitly quantifying the heat and momentum budgets. Our results suggest that the wave-feedback mechanism plays a particularly dominant role even within the first few weeks following aerosol injection. During this early period, the zonal wind anomalies are in thermal-wind balance, indicating that the stratospheric gradient mechanism is also applicable. However, our heat-budget analysis reveals that the enhanced temperature gradients are driven primarily by dynamical processes rather than by direct radiative effects.

Understanding both the initial and longer-term responses, as well as the mechanisms driving their evolution, remains an important topic for future research. For instance, the “tropospheric gradient mechanism,” which involves changes in the surface temperature gradient, was not relevant during the early adjustment period but is expected to become important later. Investigating how and when this mechanism emerges will be crucial. It will also be valuable to examine the mechanisms that sustain circulation anomalies over extended timescales—months to years after the aerosol perturbation—and to assess how the global transport of aerosols influences these responses. Further work should also investigate how the strengthening of the SPV translates into tropospheric atmospheric changes, such as the North Atlantic Oscillation as well as surface climate.

Conflict of Interest

The authors declare no conflicts of interest relevant to this study.

Availability Statement

The data used in the generation of the figures of this paper are available in Yook (2026). WACCM4 is an open-source community model, which was developed with support primarily from the National Science Foundation, see Marsh et al. (2013).

References

- Banerjee, A., Butler, A. H., Polvani, L. M., Robock, A., Simpson, I. R., & Sun, L. (2021). Robust winter warming over Eurasia under stratospheric sulfate geoengineering—the role of stratospheric dynamics. *Atmospheric Chemistry and Physics*, 21(9), 6985–6997. <https://doi.org/10.5194/acp-21-6985-2021>
- Bardeen, C. G., Kinnison, D. E., Toon, O. B., Mills, M. J., Vitt, F., Xia, L., et al. (2021). Extreme ozone loss following nuclear war results in enhanced surface ultraviolet radiation. *Journal of Geophysical Research: Atmospheres*, 126(18), e2021JD035079. <https://doi.org/10.1029/2021jd035079>
- Bardeen, C. G., Toon, O., Jensen, E., Marsh, D., & Harvey, V. (2008). Numerical simulations of the three-dimensional distribution of meteoric dust in the mesosphere and upper stratosphere. *Journal of Geophysical Research*, 113(D17), D17202. <https://doi.org/10.1029/2007jd009515>
- Bittner, M., Timmreck, C., Schmidt, H., Toohey, M., & Krüger, K. (2016). The impact of wave-mean flow interaction on the Northern Hemisphere polar vortex after tropical volcanic eruptions. *Journal of Geophysical Research: Atmospheres*, 121(10), 5281–5297. <https://doi.org/10.1002/2015jd024603>
- Coupe, J., & Robock, A. (2021). The influence of stratospheric soot and sulfate aerosols on the Northern Hemisphere wintertime atmospheric circulation. *Journal of Geophysical Research: Atmospheres*, 126(11), e2020JD034513. <https://doi.org/10.1029/2020jd034513>

Acknowledgments

S. Y. was supported by a Grant from the Future of Life Institute. J. H. was supported by Hankuk University of Foreign Studies Research Fund. The CESM project is supported primarily by the U.S. National Science Foundation. The authors acknowledge the Climate Simulation Laboratory at NCAR's Computational and Information Systems Laboratory (CISL), sponsored by NSF and other agencies) and the MIT's Massachusetts Green High Performance Computing Center (supported by the Center for Sustainability Science and Strategy) for providing computing and storage resources. Open Access funding enabled and organized by MIT Hybrid 2026. We thank Alan Robock and two anonymous reviewers for their helpful comments on the manuscript.

- DallaSanta, K., Gerber, E. P., & Toohy, M. (2019). The circulation response to volcanic eruptions: The key roles of stratospheric warming and eddy interactions. *Journal of Climate*, 32(4), 1101–1120. <https://doi.org/10.1175/jcli-d-18-0099.1>
- Dima, I. M., Wallace, J. M., & Kraucunas, I. (2005). Tropical zonal momentum balance in the NCEP reanalyses. *Journal of the Atmospheric Sciences*, 62(7), 2499–2513. <https://doi.org/10.1175/jas3486.1>
- Graf, H.-F., Li, Q., & Giorgetta, M. (2007). Volcanic effects on climate: Revisiting the mechanisms. *Atmospheric Chemistry and Physics*, 7(17), 4503–4511. <https://doi.org/10.5194/acp-7-4503-2007>
- Graft, H., Kirchner, I., Robock, A., & Schult, I. (1993). Pinatubo eruption winter climate effects: Model versus observations. *Climate Dynamics*, 9(2), 81–93. <https://doi.org/10.1007/bf00210011>
- Haigh, J. D., Blackburn, M., & Day, R. (2005). The response of tropospheric circulation to perturbations in lower-stratospheric temperature. *Journal of Climate*, 18(17), 3672–3685. <https://doi.org/10.1175/jcli3472.1>
- Holton, J. R. (2004). *An introduction to dynamic meteorology* (Vol. 88). Academic Press.
- Jones, A., Haywood, J. M., Jones, A. C., Tilmes, S., Kravitz, B., & Robock, A. (2021). North Atlantic Oscillation response in GeoMIP experiments G6solar and G6sulfur: Why detailed modelling is needed for understanding regional implications of solar radiation management. *Atmospheric Chemistry and Physics*, 21(2), 1287–1304. <https://doi.org/10.5194/acp-21-1287-2021>
- Kinnison, D., Brasseur, G. P., Walters, S., Garcia, R., Marsh, D., Sassi, F., et al. (2007). Sensitivity of chemical tracers to meteorological parameters in the MOZART-3 chemical transport model. *Journal of Geophysical Research*, 112(D20), D20302. <https://doi.org/10.1029/2006jd007879>
- Kodera, K. (1994). Influence of volcanic eruptions on the troposphere through stratospheric dynamical processes in the Northern Hemisphere winter. *Journal of Geophysical Research*, 99(D1), 1273–1282. <https://doi.org/10.1029/93jd02731>
- Kodera, K. (1995). On the origin and nature of the interannual variability of the winter stratospheric circulation in the Northern Hemisphere. *Journal of Geophysical Research*, 100(D7), 14077–14087. <https://doi.org/10.1029/95jd01172>
- Lachmy, O., & Kaspi, Y. (2020). The role of diabatic heating in Ferrel cell dynamics. *Geophysical Research Letters*, 47(23), e2020GL090619. <https://doi.org/10.1029/2020gl090619>
- Madronich, S., & Flocke, S. (1997). Theoretical estimation of biologically effective UV radiation at the Earth's surface. In *Solar ultraviolet radiation: Modelling, measurements and effects* (pp. 23–48). Springer.
- Marsh, D. R., Mills, M. J., Kinnison, D. E., Lamarque, J.-F., Calvo, N., & Polvani, L. M. (2013). Climate change from 1850 to 2005 simulated in CESM1 (WACCM). *Journal of Climate*, 26(19), 7372–7391. <https://doi.org/10.1175/jcli-d-12-00558.1>
- Mills, M. J., Toon, O. B., Lee-Taylor, J., & Robock, A. (2014). Multidecadal global cooling and unprecedented ozone loss following a regional nuclear conflict. *Earth's Future*, 2(4), 161–176. <https://doi.org/10.1002/2013ef000205>
- Mills, M. J., Toon, O. B., Turco, R. P., Kinnison, D. E., & Garcia, R. R. (2008). Massive global ozone loss predicted following regional nuclear conflict. *Proceedings of the National Academy of Sciences of the United States of America*, 105(14), 5307–5312. <https://doi.org/10.1073/pnas.0710058105>
- Newman, P. A., Nash, E. R., & Rosenfield, J. E. (2001). What controls the temperature of the Arctic stratosphere during the spring? *Journal of Geophysical Research*, 106(D17), 19999–20010. <https://doi.org/10.1029/2000jd000061>
- Pausata, F. S., Lindvall, J., Ekman, A. M., & Svensson, G. (2016). Climate effects of a hypothetical regional nuclear war: Sensitivity to emission duration and particle composition. *Earth's Future*, 4(11), 498–511. <https://doi.org/10.1002/2016ef000415>
- Robock, A., & Mao, J. (1995). The volcanic signal in surface temperature observations. *Journal of Climate*, 8(5), 1086–1103. [https://doi.org/10.1175/1520-0442\(1995\)008<1086:tvssist>2.0.co;2](https://doi.org/10.1175/1520-0442(1995)008<1086:tvssist>2.0.co;2)
- Robock, A., Oman, L., & Stenchikov, G. L. (2007). Nuclear winter revisited with a modern climate model and current nuclear arsenals: Still catastrophic consequences. *Journal of Geophysical Research*, 112(D13), D13107. <https://doi.org/10.1029/2006jd008235>
- Simpson, I. R., Blackburn, M., & Haigh, J. D. (2009). The role of eddies in driving the tropospheric response to stratospheric heating perturbations. *Journal of the Atmospheric Sciences*, 66(5), 1347–1365. <https://doi.org/10.1175/2008jas2758.1>
- Stenchikov, G., Robock, A., Ramaswamy, V., Schwarzkopf, M. D., Hamilton, K., & Ramachandran, S. (2002). Arctic Oscillation response to the 1991 Mount Pinatubo eruption: Effects of volcanic aerosols and ozone depletion. *Journal of Geophysical Research*, 107(D24), ACL28-21–ACL28-16. <https://doi.org/10.1029/2002jd002090>
- Toohy, M., Krüger, K., Bittner, M., Timmreck, C., & Schmidt, H. (2014). The impact of volcanic aerosol on the Northern Hemisphere stratospheric polar vortex: Mechanisms and sensitivity to forcing structure. *Atmospheric Chemistry and Physics*, 14(23), 13063–13079. <https://doi.org/10.5194/acp-14-13063-2014>
- Toon, O. B., Bardeen, C. G., Robock, A., Xia, L., Kristensen, H., McKinzie, M., et al. (2019). Rapidly expanding nuclear arsenals in Pakistan and India portend regional and global catastrophe. *Science Advances*, 5(10), eaay5478. <https://doi.org/10.1126/sciadv.aay5478>
- Waugh, D. W., Sobel, A. H., & Polvani, L. M. (2017). What is the polar vortex and how does it influence weather? *Bulletin of the American Meteorological Society*, 98(1), 37–44. <https://doi.org/10.1175/bams-d-15-00212.1>
- White, I. P., Lachmy, O., & Harnik, N. (2024). Influence of a local diabatic heating source on the midlatitude circulation. *Quarterly Journal of the Royal Meteorological Society*, 150(765), 5167–5187. <https://doi.org/10.1002/qj.4863>
- Yook, S. (2026). Replication data for: Figures in Northern Hemisphere wintertime stratospheric circulation response to smoke injection from a regional nuclear conflict [Dataset]. *Harvard Dataverse*. <https://doi.org/10.7910/DVN/GX8OGB>
- Yook, S., Solomon, S., Bardeen, C. G., & Stone, K. (2025). Arctic ozone hole and enhanced mid-latitude ozone losses due to heterogeneous halogen chemistry following a regional nuclear conflict. *Earth's Future*, 13(12), e2025EF006866. <https://doi.org/10.1029/2025ef006866>

References From the Supporting Information

- Andrews, D. G., Leovy, C. B., & Holton, J. R. (1987). *Middle atmosphere dynamics* (Vol. 40). Academic Press.
- Haynes, P. H., McIntyre, M. E., Shepherd, T. G., Marks, C. J., & Shine, K. P. (1991). On the “downward control” of extratropical diabatic circulations by eddy-induced mean zonal forces. *Journal of the Atmospheric Sciences*, 48(4), 651–680. [https://doi.org/10.1175/1520-0469\(1991\)048<0651:OTCOED>2.0.CO;2](https://doi.org/10.1175/1520-0469(1991)048<0651:OTCOED>2.0.CO;2)
- Vallis, G. K. (2006). *Atmospheric and Oceanic fluid dynamics: Fundamentals and large-scale circulation* (p. 561). Cambridge University Press.